A Potential Study on Radio Tomography to Localize the Moisture Distribution in Rice Silo

N. A. M. Ramli[1,3], M. H. F. Rahiman[1*,3], L. M. Kamarudin[2,3], L. Mohamed[1,3], and A. Zakaria[1,3]

[1*] Faculty of Electrical Engineering Technology, Universiti Malaysia Perlis, Pauh Putra Campus, 02600 Arau, Perlis, Malaysia
[2] Faculty of Electronic Engineering Technology, Universiti Malaysia Perlis, Pauh Putra Campus, 02600 Arau, Perlis, Malaysia
[3] Centre of Excellence for Advance Sensor Technology (CEASTech), Universiti Malaysia Perlis, Pauh Putra Campus, 02600 Arau, Perlis, Malaysia

Corresponding author* email: hafiz@unimap.edu.my
Accepted 3 March 2021, available online 31 March 2021

ABSTRACT

As the rice grains are naturally hygroscopic, their quality post-harvesting revolves around their level of moisture content. In Malaysia, it is challenging to maintain and preserve the rice quality for long-term storage due to our hot, humid climate with a relative humidity of approximately 80%. Besides, the current moisture measurement method is unreliable because it is a single-point assessment, whereas the moisture build-up inside the rice silo is indefinite. In this manuscript, we proposed a radio tomography system capable of localizing the moisture distribution inside the silo. Radio tomography is a well-known technology for its imaging generated based on the attenuated radio signals caused by the objects within the wireless sensor network. Several positions of moisture profile were simulated to evaluate the performance of the system. The reconstructed image using both LBP and FBP algorithms has established the findings where the approach adequately reconstructs the 2D images of the moisture profiles.

Keywords: Radio tomography, Rice moisture content, Rice silo, Image reconstruction

1. Introduction

Rice is a whole grain primarily composed of carbohydrates, and it is mostly consumed to fulfil the range of nutrient intakes and energy supplies. In Malaysia, the growing demand for rice grain [1] has required it to be properly stored for a varying period of time without losing its quality. However, like any other grain crops, rice can also be easily deteriorated if it is exposed to inappropriate storage environment, which could lead to shorten its shelf life [2], [3]. Hence, proper post-harvest rice storage is necessary to preserve its overall quality from damage caused by inclement weather, moisture build-up, and microbial development such as fungi and insects [4]–[7].

Rice storage systems can be classified in many forms depending on the quantity of grains to be stored, the purpose of storage, and the location of the warehouse. To acknowledge the major factor required for a good storage, literatures have described that the rice silo should prevent the moisture build-up or re-entering the grains after the drying process [8]–[11]. According to [12], the optimal level of moisture content required to control progressive changes in the physicochemical properties of the rice grains is around 14% or less respective to their storage period. Moisture content is referred to the total weight of the grain, including the water expressed in percentage.

Nowadays, the grain moisture content is being measured by using the primary and secondary method. The primary method [13] is sensing the absolute moisture in grain through the standard oven drying process. While the second method is more straightforward and convenient [14], that works based on the relationship between grains' moisture content and the dielectric properties of the grain [15]. Although the revolution of the moisture meter provides rapid measurement, it is impractical to be applied since it is typically destructive, and the single-point measurement did not represent the location of the moisture distribution for the whole grain in the silo.

Therefore, an inclusive moisture measurement method is essential to supervise the moisture distribution inside the rice silo. We proposed a potential study on a radio tomography method, which perhaps could localize the area of higher moisture distribution within the rice silo. Radio frequency (RF) signal is known to have some level of sensitivity towards moisture [16]. This characteristic can be exploited to localize the source of the moisture build-up in the form of tomogram and thus, make it possible to provide a full spectrum of moisture distribution inside the silo. This method is certainly innovative, inclusive and non-destructive.

2. Methodology

The percentage of moisture content (MC) is calculated based on the attributed grain dielectric properties [17]. The first recorded data that illustrate the correlation between grain dielectric properties with MC was presented by [18]. Dielectric properties are the electrical characteristics of poorly conducting materials that can be polarized by an electric field. Their influences in absorption and dissipation of electromagnetic energy, when subjected to radio frequency, is therefore significant for moisture sensing in the agricultural industry.

Based on these features, we introduced a radio tomographic imaging to assess the moisture distribution inside a rice silo. RTI system has drawn wide recognition since the targeted object does not need to carry tracking devices to be detected. Its basic principle is that, within a wireless sensor network, when an object obstructs the transmission links, the quality of the associated links would attenuate, while the unblock links keep unchanged. Figure 1 below demonstrates a 2D concept of the RTI system simulated in a finite element modelling (FEM) study.

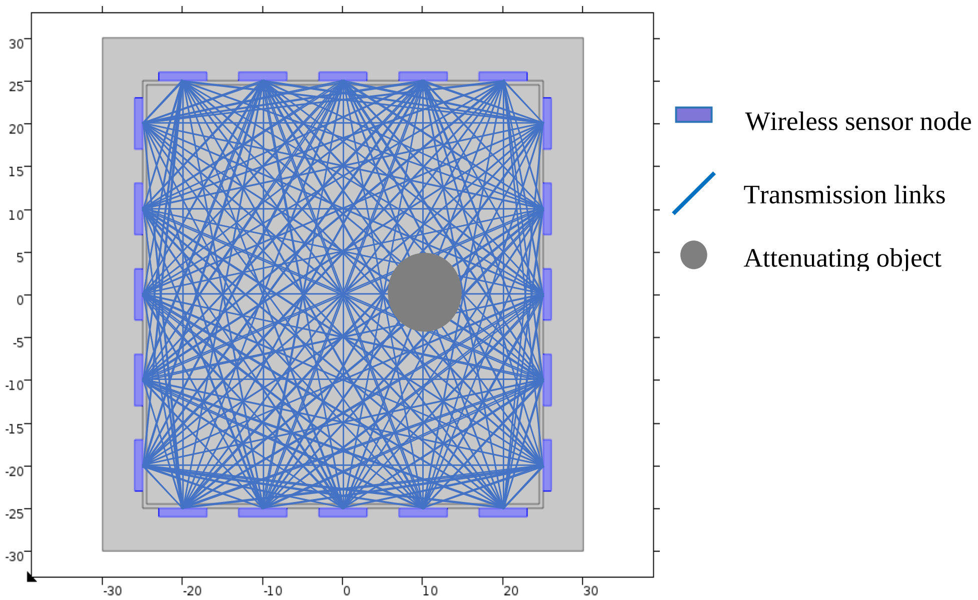

Figure. 1. Illustration of an RTI system

2.1 Radio Frequency Sensing of Dielectric Properties

This RTI system is based on the relationship between the radio frequency and the material's dielectric properties. The properties of the medium, also known as relative complex permittivity, are expressed in Eq. (1).

$$\varepsilon = \varepsilon' - j\varepsilon'' \tag{1}$$

where ε' is the dielectric constant that describes the capability of a material to store energy in the electric field, and ε'' is the dielectric loss factor that indicates the capability of a material to dissipate energy from the electric field, which is then being converted into heat energy. Eq. (2) below defines the material's conductivity.

$$\sigma = \omega\varepsilon_o\varepsilon'' \tag{2}$$

where $\omega = 2\pi f$ is the angular frequency with f in Hz, and ε_o is the permittivity of free space which is equivalent to 8.854×10^{-12} F/m.

The nature of the correlation in dielectric properties and changes in MC of rice grains is better illustrated by [19]. One can see that, at any applied frequency, the dielectric constant, $\boldsymbol{\varepsilon'}$ almost linearly correlated to rice grains MC, while loss factor, $\boldsymbol{\varepsilon''}$ is found to be less predictable. Herein, the modelling of the medium's dielectric properties is separated into two parts, which are the dried rice and rice moisture phantom. It is because the main objective of this research is to facilitate moisture distribution. The dried rice medium (reference medium) was assumed to be at 14% MC based on the standard level of MC for rice grain storage. For the rice moisture phantom, they were adopted to be at 28% MC to manifest the worst condition for the rice grains since the maximum MC of rice grains post-harvesting is about 25% [12]. Their modelling of dielectric properties was retrieved according to [20].

2.2 Radio Tomographic Imaging (RTI) Approach

The main objective of this work is to investigate the potential of using a radio tomographic imaging (RTI) system to reconstruct the tomograms of rice moisture distribution inside a silo. A configuration of an FEM simulation was modelled to study the behaviour of radio frequency (RF) and evaluate the performance of the RTI system. The schematic diagram of the RTI system is, as shown in figure 2. The selected geometrical dimension, number of RF nodes, and dielectric properties of each domain need to be taken into consideration because different development phase would have modified the behaviour and distribution of the electromagnetic field.

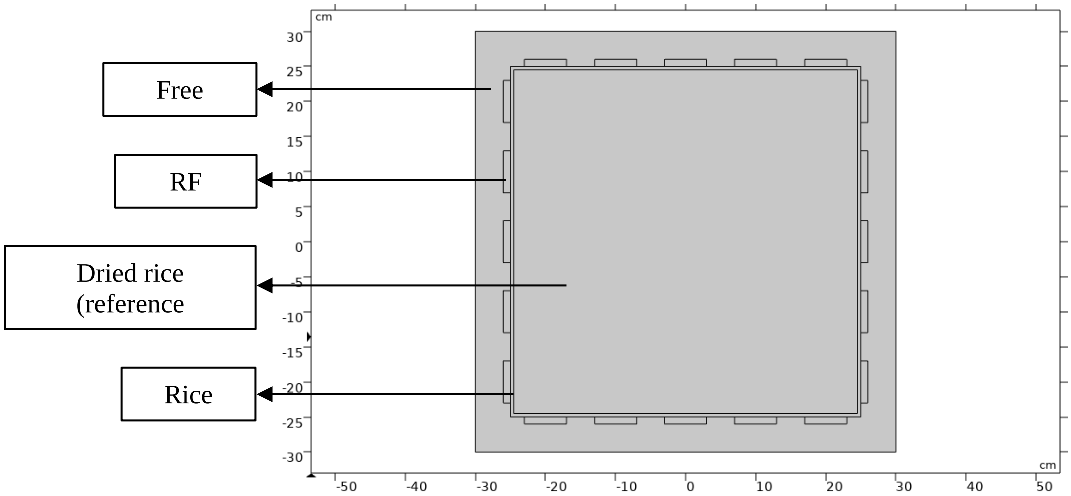

Figure. 2. Configuration of the RTI system

The RTI system is composed of 20 RF nodes equally arrayed along the perimeter of 0.5 m × 0.5 m square silo, with an operating frequency of 2.4 GHz. The RF node was set as transceivers, which continuously measure the change in the electric field within the monitored area introduced by the presence of rice moisture phantoms (refer figure 4). The width of the node, $\boldsymbol{w}$ is calibrated using Eq. (3) [21]. The cut-off frequency, $\boldsymbol{f_c}$ was calculated by substituting the desired width, $\boldsymbol{w}$ and the relative permittivity, $\boldsymbol{\varepsilon_r}$ of the reference medium. If the cut-off frequency is lower than the operating frequency, the RF signals can propagate in the reference medium.

$$\boldsymbol{f_c = \frac{c_o}{2w\sqrt{\varepsilon_r}}} \tag{3}$$

where $\boldsymbol{c_o}$ is the speed of light in a vacuum, $\boldsymbol{c_o = 3 \times 10^8}$ ms^{-1}.

The rice silo used in this simulation study is made up of acrylic plates with a thickness of 10 mm. It is designed initially for the purpose to test the capability of the RTI system to image the higher MC inside the silo. Logically, the bigger the silo size, the higher the attenuation of the electromagnetic waves [22]. Lastly, the transmission power used was restricted to 1 mW. The restriction was set to prevent any changes in the dielectric properties of the rice grains due to RF heating [23], and the temperature is a critical factor affecting the physicochemical properties of the rice [24]. The parameters used in this FEM study are summarized in Table 1.

Table 1. MSSIM indexes calculated on the reconstructed images

Parameters	Values
Number of RF nodes	20
RF nodes' width	0.06 m
Operating frequency	2.4 GHz
Power	1 mW
Domain size (air)	0.6 m × 0.6 m
Silo size	0.5 m × 0.5 m
Dielectric properties of dried rice	Conductivity: 0.0803 S/m
	Relative permittivity: 3.6384
Dielectric properties of rice moisture phantom	Conductivity: 0.7738 S/m
	Relative permittivity: 26.2104

2.3 Solving Forward Problem

The forward problem is assessed so that the sensitivity map of the theoretical scattered electromagnetic field at each sensor node can be obtained. Sensitivity map is the projection effect of a particular node to a known receiving node in terms of weighting matrices where the matrices represent the attenuation of the electric field [25]. The basic linear formulation model was applied, and the transmission links are considered reciprocity, where the transmission links between node 1 and 2 and that between 2 and 1 would be the same [26]. Thus, with 20 nodes deployed, the maximum number of measured radio links would be 190. The discretized electric field strength was solved based on the distribution of the dielectric properties of dried rice, rice phantom with 28% MC, and the excitation of electromagnetic energy in terms of frequency [21]. This approach is possible since the dielectric properties are capable of manipulating the behaviour of the electromagnetic field, which have been proven by [27].

Figure 3 (a) describes the meshing scheme of the RTI system for Phantom D (see figure 4). Extra fine mesh size is used with the maximum element size of 1.2 cm and the minimum element size of 0.0045 cm, and the same mesh size is used for the case without the rice moisture phantoms. In this FEM electromagnetic solver, the meshing is computed with different parameters for each domain to get a uniform approximation to the actual solution, and finer meshing near the nodes, where more accuracy is needed [28]. Figure 3 (b) illustrates the computation of the total electric field, E^{tot} on Phantom D when RF node 3 is radiating. Simultaneously, the incident electric field, E^{inc} by the forward solver is the electric field when rice moisture phantom is absent in the reference medium (dried rice context). Eq. (4) shows the relationship between the total electric field and the incident electric field.

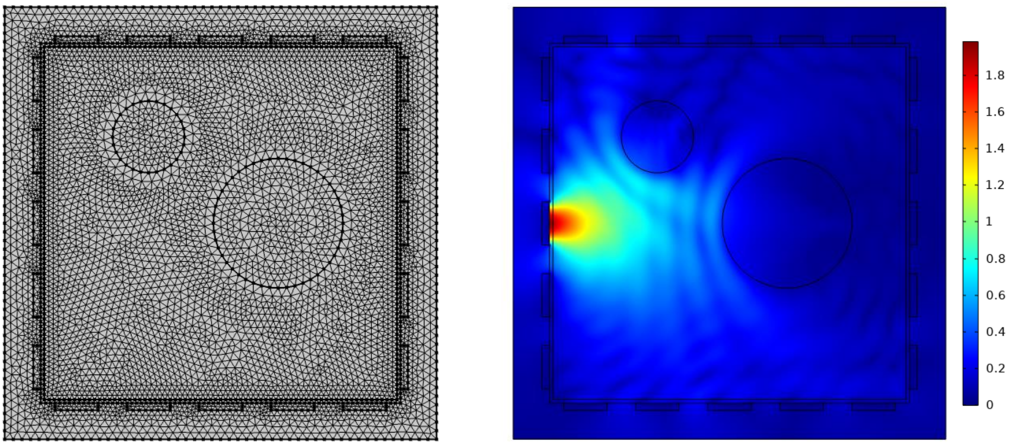

(a) Mesh scheme of the RTI

(b) Normalized electric field when RF node 3 is radiating at 2.4 GHz

Figure. 3. (a) Mesh scheme of the RTI system (b) Normalized electric field when RF node 3 is radiating

$$E^{tot} = E^{inc} + E^{sca} \tag{4}$$

where E^{sca} is the scattered electric field.

The analysis and mapping of the scattered electric field E^{sca} were accomplished by coding the algorithm for image reconstruction through MATLAB. The number of pixels that reflect the image's resolutions was set to 600 × 600 pixels.

2.4 Solving Inverse Problem

The attempts of image reconstruction in the RTI system is to solve the ill-posed inverse problem because it is the essence of soft-field tomography where small noises in the measurement data are enhanced to the point that the images are insignificant [26]. By solving the inverse problem, the unknown electric field distribution vector in the computational domain can be determined using the image reconstruction algorithm. In this work, Linear Back Projection (LBP) and Filtered Back Projection (FBP) algorithms have been proposed to address this tomographic problem.

LBP algorithm is well known for its simple computational procedure which enables it to generate an image at high speed [29]. Through the LBP algorithm, each sensitivity matrix is multiplied with its corresponding sensor loss [25]. Although the LBP algorithm produces smearing effects, it has been able to meet the basic requirement of scenarios such as localization. In the FBP algorithm, a filter matrix F is introduced to sharpen the reconstructed image acquired from the LBP algorithm [30]. The filter matrix F is attained by dividing the maximum pixel magnitude in overall sensitivity, P_m with the total sensitivity matrix W. Then, the FBP algorithm can be expressed by multiplying the filter matrix F with the concentration profiles obtained by the LBP algorithm.

$$G_{LBP}(x,y) = \sum_{Tx=1}^{N} \sum_{Rx=1}^{N} \bar{M}_{Tx,Rx}(x,y) \times S_{Tx,Rx} \tag{5}$$

$$G_{FBP}(x,y) = F(x,y) \times G_{LBP}(x,y) \tag{6}$$

$$F = \frac{P_m}{W} \tag{7}$$

$$W = \sum_{Tx=1}^{20} \sum_{Rx=1}^{20} M_{Tx,Rx} \tag{8}$$

where N is the number of RF nodes, $\bar{M}_{Tx,Rx}(x,y)$ is the normalized sensitivity matrix in view of T_x and R_x, $S_{Tx,Rx}$ is the sensor loss at R_x^{th} for projection T_x^{th}, $G_{LBP}(x,y)$ is the LBP concentration profile, and $G_{FBP}(x,y)$ is the FBP concentration profile.

3. Results and Discussion

In this section, the results of the FEM simulations were presented to investigate if the approaches are proficient to be employed in the RTI system. The study was done based on the designated test profiles, background's value and assigned frequency; and each profile was reconstructed by solving the inverse problems using linear image algorithm LBP and FBP. The dissimilar scenarios of moisture distribution at 28% MC were arbitrarily constructed to act as the general representative upon simulating the rice moisture phantoms. Table 2 illustrates the reconstructed images using LBP and FBP algorithms, where the highest and lowest contrast are indicated in red and blue, respectively.

Consequently, the performance was being analyzed by executing an image quality assessment, Mean Structural Similarity Index (MSSIM) calculation on the four different profiles. The output MSSIM index is in the range 0 to 1, where the higher the index, the closer the reconstructed image to the reference image. The following MSSIM indexes were tabulated and discussed as in table 3 and figure 5.

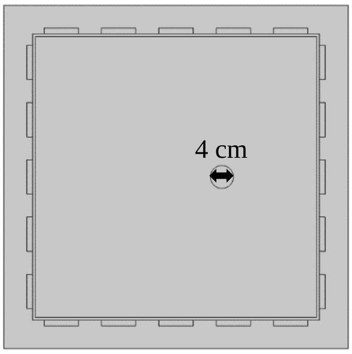

(a) Phantom A

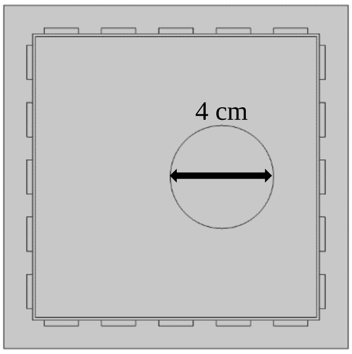

(b) Phantom B

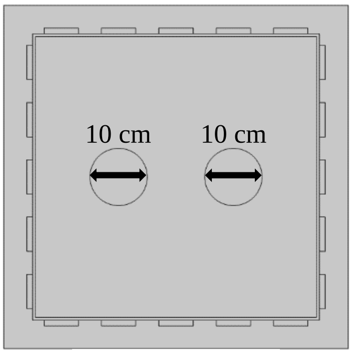

(c) Phantom C

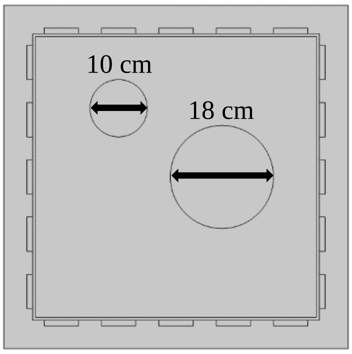

(d) Phantom D

Figure. 4. Simulation of rice moisture phantoms

Table 2. Reconstructed image for Phantom A, B, C, and D using LBP and FBP algorithms

Phantom	Reference image	LBP	FBP
A	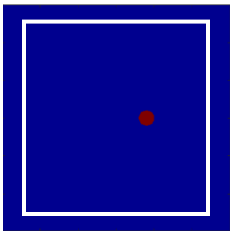	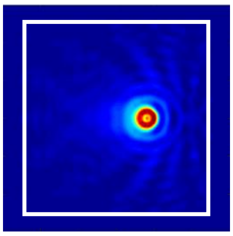	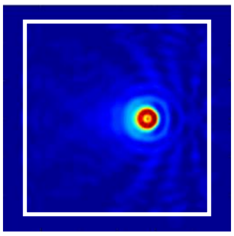
B	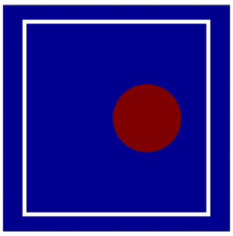	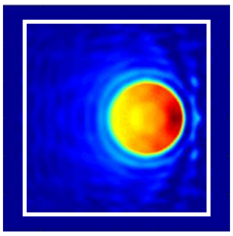	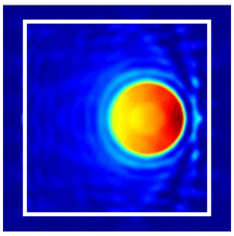
C	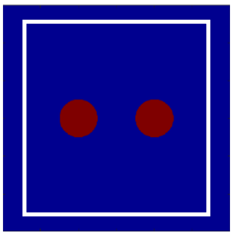	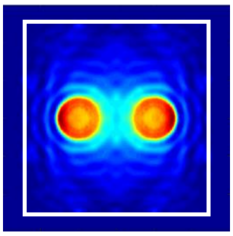	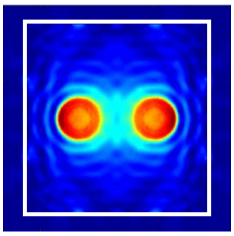
D	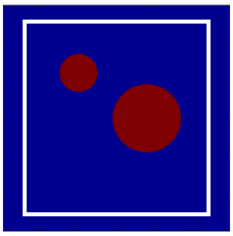	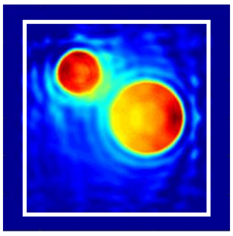	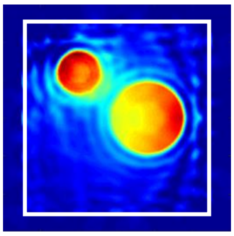

From Table 2, the overall findings presented that the simulation results constructed by both LBP and FBP algorithms provide significant information where all the rice moisture phantoms could be identified and distinguished from the dried rice context. Based on the reconstructed image of Phantom A, both LBP and FBP algorithms possessed a result corresponding to the real image phantom as small as 4 cm diameter. Besides, for Phantom C, when there was a duplicated phantom with a distance of 10 cm from each other, this technique successfully reconstructed the image, despite the presence of smearing effects. By looking at Phantom D, at different size and position, the rice moisture phantoms could still be clearly recognized and reconstructed by both algorithms.

According to the image tabulated, the size of the moisture phantoms slightly reformed. It was assumed that the high contrast of dielectric properties between dried rice and rice phantom would cause a small re-polarization to the initial field of an incident electromagnetic field. However, the general outcome shows some promising evidence to support the possibility of using RTI system for rice moisture localization.

Table 3. MSSIM indexes calculated on the reconstructed images

Phantom	LBP	FBP
A	0.4875	0.3956
B	0.4005	0.2653
C	0.3758	0.2487
D	0.4029	0.2855

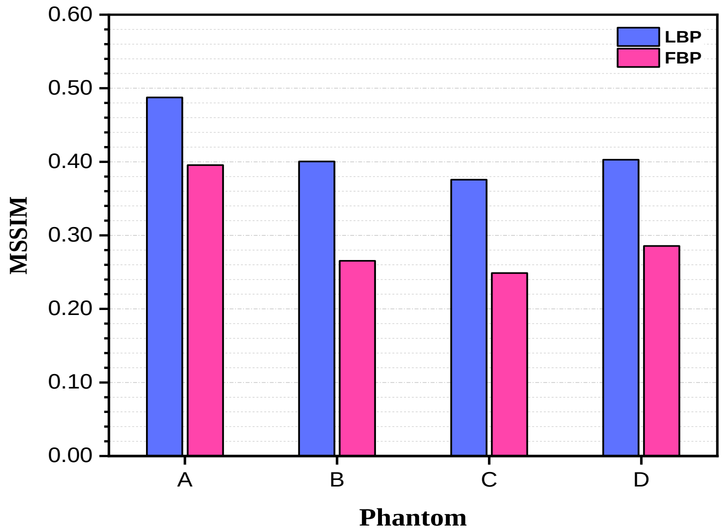

Figure. 5. MSSIM index graphs computed on the reconstructed images

Table 3 and figure 5 clearly demonstrated the MSSIM assessment calculated by comparing the reconstructed image with the reference image. The highest and lowest MSSIM index scored by the algorithm LBP is 0.4875 for Phantom A and 0.3758 for Phantom C, respectively. Whereas, for MSSIM index scored by the algorithm FBP, Phantom A gave the highest index at 0.3956 while the lowest is scored by Phantom C, at index 0.2487.

Based on the results, moderate MSSIM indexes were obtained for all phantom profiles. It can be observed that algorithm LBP recorded higher MSSIM indexes for all phantoms' conditions. We believed that the ill-posedness of the RTI behaviour had given the FBP algorithm a lower quality of image reconstructed, particularly when the filter matrix is multiplied with the LBP result. Hence, it can be deduced that the applied LBP algorithm is better in reconstructing the moisture distribution in the rice silo compared to the FBP algorithm.

4. Conclusion

In this initial study, the potentiality of using radio tomography for rice moisture distribution sensing was adequately performed. The simulation results of the proposed technique are shown in terms of the image depicted along with the assessment using MSSIM index. The quantitative and MSSIM analysis has established the findings and apparently, the reconstructed rice moisture phantoms have an almost similar shape, size and location as compared to the corresponding real phantoms. This evaluation makes it possible to certify the capability of an RTI system in monitoring the location of the moisture distribution, which perhaps it could provide a more practical approach over conventional methods. However, concerning an actual case study, further research work should be done to explore the reliability, sensitivity towards the moisture changes, the effectiveness of the proposed reconstruction algorithms as well as the validity of the image quality assessment.

Acknowledgement

The authors would like to thank the Ministry of Higher Education Malaysia for funding this research under the Transdisciplinary Research Grant Scheme (Ref: TRGS/1/2018/UNIMAP/02/4/2). Special acknowledgement indeed goes to Universiti Malaysia Perlis for the facilities and technical support.

References

[1] Omar, S. C., Shaharudin, A., & Tumin, S. A. (2019). The status of the paddy and rice industry in Malaysia. Khazanah Research Institute. Kuala Lumpur.
[2] Pekmez, H. (2016). Cereal storage techniques: a review. *J. Agric. Sci. Technol. B*, *6*, 67–71.
[3] Saikrishna, A., Dutta, S., Subramanian, V., Moses, J. A., & Anandharamakrishnan, C. (2018). Ageing of rice: A review. *Journal of Cereal Science*, *81*, 161–170.
[4] Wang, W., He, A., Peng, S., Huang, J., Cui, K., & Nie, L. (2018). The effect of storage condition and duration on the deterioration of primed rice seeds. *Frontiers in plant science*, *9*, 172.

[5] Espino, L., Greer, C., Mutters, R., & Thompson, J. (2014). Survey of rice storage facilities identifies research and education needs. *California Agriculture*, *68*(1), 38–46.
[6] Park, C. E., Kim, Y. S., Park, K. J., & Kim, B. K. (2012). Changes in physicochemical characteristics of rice during storage at different temperatures. *Journal of stored products research*, *48*, 25–29.
[7] Bartosik, R. (2012, October). An inside look at the silo-bag system. In *Proc 9th. Int. Conf. on Controlled Atmosphere and Fumigation in Stored Products, Antalya, Turkey* (15–19).
[8] Alhendi, A. S., Al-Rawi, S. H., & Jasim, A. M. (2019). Effect of moisture content of two paddy varieties on the physical and cooked properties of produced rice. *Brazilian Journal of Food Technology*, *22*.
[9] Shafiekhani, S., Wilson, S. A., & Atungulu, G. G. (2018). Impacts of storage temperature and rice moisture content on color characteristics of rice from fields with different disease management practices. *Journal of stored products research*, *78*, 89–97.
[10] Naik, D. S., & Chetti, M. B. (2017). Influence of packaging and storage condition on the moisture content and its effect on fungal load of paddy. *Research Journal of Agricultural Science*, *8*(2), 370–374.
[11] Putri, R. E., Yahya, A., Adam, N. M., & Aziz, S. A. (2015). Related fracture resistance with moisture content in different grain orientation of paddy grain. *J. Biol. Agric. Healthc.*, 5.
[12] Postharvest C., "Grain Storage and Pest Management, (2013). [Online]. Available: postharvest@irri.org.
[13] Klomklao, P., Kuntinugunetanon, S., & Wongkokua, W. (2017, September). Moisture content measurement in paddy. In *Journal of Physics: Conference Series*, *901*(1), p. 012068). IOP Publishing.
[14] Zambrano, M. V., Dutta, B., Mercer, D. G., MacLean, H. L., & Touchie, M. F. (2019). Assessment of moisture content measurement methods of dried food products in small-scale operations in developing countries: A review. *Trends in Food Science & Technology*, *88*, 484–496.
[15] Nelson, S. (2015). *Dielectric properties of agricultural materials and their applications*. Academic Press.
[16] Zhang, C., Zhou, X., Shi, Z., & Wang, L. (2017, December). A novel method for measuring the moisture distribution of grain in the silo based on microwave image technology. In *2017 International Conference on Advanced Mechatronic Systems (ICAMechS)* (157–162). IEEE.
[17] Mbie N. Z. (2017). *APLMF Guide Document on Rice Moisture Measurement*.
[18] Nelson, S. O. (1965). Dielectric properties of grain and seed in the 1 to 50–mc range. *Transactions of the ASAE*, *8*(1), 38-0048.
[19] Mun, H. K., You, K. Y., & Dimon, M. N. (2015). Rice grain moisture determination using microstrip wide-ring and microstrip coupled-line sensors. *American Journal of Applied Sciences*, *12*(2), 112.
[20] You, K. Y., You, L. L., Yue, C. S., Mun, H. K., & Lee, C. Y. (2017). Physical and chemical characterization of rice using microwave and laboratory methods. *Rice; IntechOpen: London, UK*, 81–99.
[21] Mallach, M., Gebhardt, P., & Musch, T. (2017). 2D microwave tomography system for imaging of multiphase flows in metal pipes. *Flow Measurement and Instrumentation*, *53*, 80–88.
[22] Hu, G. (2016). Study on the Signal Transmission Characteristics of 2.4 GHz Wireless Network in Dorms. *International Journal of Online Engineering*, *12*(10).
[23] Baker-Jarvis, J., & Kim, S. (2012). The interaction of radio-frequency fields with dielectric materials at macroscopic to mesoscopic scales. *Journal of research of the National Institute of Standards and Technology*, *117*, 1.
[24] Siwar, C., Idris, N. D. M., Yasar, M., & Morshed, G. (2014). Issues and challenges facing rice production and food security in the granary areas in the East Coast Economic Region (ECER), Malaysia. *Research Journal of Applied Sciences, Engineering and Technology*, *7*(4), 711–722.
[25] Mohd. Hafiz Fazalul Rahiman. (2013). *Ultrasonic tomography system for liquid/gas bubble column* (Doctoral dissertation, Universiti Teknologi Malaysia).
[26] Wilson, J., & Patwari, N. (2010). Radio tomographic imaging with wireless networks. *IEEE Transactions on Mobile Computing*, *9*(5), 621-632.
[27] Mazima, J. K., Johnson, A., Manasseh, E., & Kaijage, S. (2018). An overview of electromagnetic radiation on grain crops. *Food Science and Technology: An International Journal*, *1*(1), 21–32.
[28] Zimam, M. A., Mohamad, E. J., Rahim, R. A., & Ling, L. P. (2011). Sensor modeling for an electrical capacitance tomography system using COMSOL Multiphysics. *Jurnal Teknologi*, 33–47.
[29] Heng, L., Zheng-huan, W., Xiang-yuan, B., & Jian-ping, A. (2012, May). Image reconstruction algorithms for radio tomographic imaging. In *2012 IEEE International Conference on Cyber Technology in Automation, Control, and Intelligent Systems (CYBER)* (48–53). IEEE.
[30] Wahab, Y. A. (2017). Inverse Problem: Comparison between Linear Back-Projection Algorithm and Filtered Back-Projection Algorithm in Soft-Field Tomography. *International Journal of Integrated Engineering*, *9*(4).